



Novel hybrid scaffold for improving the wound repair process: evaluation of combined chitosan/eggshell/vitamin D scaffold for wound healing

Azam Deilami¹ · Zahra Niknam² · Ali Golchin³ · Vahid Niazi⁴ · Hakimeh Zali^{2,4} · Meisam Omid⁵

Received: 15 January 2021 / Revised: 31 March 2021 / Accepted: 5 April 2021

© The Author(s), under exclusive licence to Springer-Verlag GmbH Germany, part of Springer Nature 2021

Abstract

The current design requirement of cutaneous wound healing is an ideal wound dressing via biodegradable property through which fibroblasts can support, migrate and proliferate. This study aimed to evaluate the effect of the synthesized hybrid scaffold based on chitosan polymer and a natural source of calcium (Ca) and vitamin D on wound healing. To achieve this purpose, three scaffolds include in chitosan (CS), eggshell + chitosan (ES/CS) and chitosan + eggshell + vitamin D (CS/ES/Vit D) were fabricated using the freeze-drying approach. Synthesized scaffolds were characterized by field emission scanning electron microscopy (FESEM), Fourier transformed infrared (FTIR), X-ray diffraction (XRD) and MTT assay. Histological examinations of the wound healing were performed using hematoxylin–eosin (H&E) and Masson's trichrome staining methods on different days in the rat full-thickness skin wound model. Finally, the effect of the synthesized scaffold was evaluated on the TGF- β 1 gene expression. The results of the scaffold characterization showed that scaffolds have the homogeneity structure. The MTT assay indicated that the cultured fibroblasts on the ES/CS and Vit D/ES/CS scaffold had viability higher than those cultured on CS. Also, histological studies demonstrated an increased effect on epithelialization and collagen production and accelerated wound healing using designed scaffolds. The TGF- β 1 gene expression in all scaffolds was

✉ Hakimeh Zali
hakimehzali@gmail.com; h.zali@sbmu.ac.ir

¹ Department of Molecular and Cellular Science, Faculty of Advanced Science & Technology, Pharmaceutical Science Branch, Islamic Azad University, Tehran, Iran

² Proteomics Research Center, Shahid Beheshti University of Medical Science, Tehran, Iran

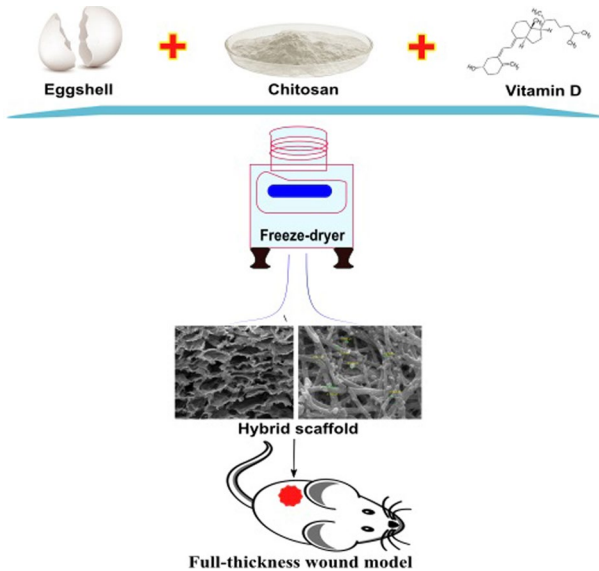
³ Department of Clinical Biochemistry and Applied Cell Sciences, School of Medicine, Urmia University of Medical Sciences, Urmia, Iran

⁴ School of Advanced Technologies in Medicine, Shahid Beheshti University of Medical Sciences, Tehran, Iran

⁵ School of Dentistry, Marquette University, Wisconsin, USA

not significantly different between test groups and controls. In general, it can be concluded that the synthesized scaffolds have the potential to accelerate wound healing and can be used as a suitable scaffold in wound management and skin regeneration.

Graphic abstract



Keywords Chitosan · Eggshell · Hydroxyapatite · Vitamin D · Wound healing · Scaffold

Introduction

Wound healing is a series of regulated biological processes including inflammation, fibroplasia, angiogenesis, form new collagen fibers, epithelialization, migration of various types of cells, production of granulated tissue and wound contraction. These require a synergistic interaction between inflammatory cells, fibroblasts, keratinocytes, biochemical intermediates and extracellular matrix molecules [1]. There are multiple growth factors at the site of the wound such as the platelet-derived growth factor (PDGF), the transforming growth factor (TGF), the epidermal growth factor (EGF) and the fibroblast growth factor (FGF), which have biological activity to stimulate the inflammatory cells infiltration to the wound area. These growth factors lead to increased keratinocytes and fibroblasts proliferation and contribute to the genesis of new capillaries in the granulated tissue and the deposition of the extracellular matrix and reconstruction wound region. It is also claimed that topical use of growth factors has succeeded in accelerating the complete wound healing in normal rats [2].

The use of natural materials in recent years has considered instead of chemicals with side effects. The most important characteristics of chitin and chitosan (CS) include high biocompatibility, biodegradability and nontoxicity regarded as safe for human dietary use and approved for wound dressing applications [3]. Besides, biological properties such as adhesion, anticancer, antimicrobial, reducing inflammation and pain and antioxidant properties, as well as blood coagulant and cholesterol-lowering agents have differentiated them from other biological polymers [4, 5]. The eggshell (ES) is a natural source of calcium (Ca) as well as collagen, ovotransferrin, ovalbumin, chondroitin sulfate, hyaluronic acid and various amino acids, which are widely used in biomedical applications, such as skin grafting, tissue displacement products, plastic surgery, corneal repair, prosthesis, implants and others [6–10]. Vitamin D, eggshell and CS are among the natural compounds that have been studied recently as factors affecting wound healing and their positive effects have been verified. Vitamin D is other biofactors that made one of the polytrophic molecules that not only has extensive effects on calcium homeostasis but also plays a role in cell differentiation, proliferation and immune response [3]. Vitamin D besides its effects on inflammatory events induces to express antimicrobial peptides and potentially enhances wound healing and protection against infections [3].

The present study attempted to find new and more effective compounds by combining CS, ES and vitamin D for improving the wound healing process. Here, the structure and biocompatibility of designed scaffolds and their effects on full-thickness wound healing in a rat model were investigated. Also, the effect of these scaffolds was examined on the TGF- β 1 gene expression with the hope of achieving a suitable and effective drug combination for wound healing.

Materials and methods

Fabrication of eggshell-derived hydroxyapatite

The egg-shells powder was produced according to our last reported approach¹. Briefly, the Gallus egg-shells were collected and washed in acetic acid (Merck, Darmstadt, Germany) (5%), ethanol (Parsmedico, Iran) (80%) and deionized water, respectively. After cleaning, the egg-shells were ground using ball milling machine. Then, the powder was sieved using a 100 μ m strainer. The powder was reacted with ortho-phosphoric acid (weight ratio = 1:5) for 24 h. The resulting product was dried at 100 °C for 12 h.

Preparation of polymer blends

To prepare polymer blends, 1 g of CS (Merck, Darmstadt, Germany) medium dissolved in 10 ml of acetic acid (1%v/v) and reached a final volume of 100 ml. Then the solution placed on a stirrer for 24 h. In the next step, three different solutions prepared according to the following; Solution A (CS): contained only a CS solution and 12.5 ml of the tween (20). Solution II (ES/CS): by adding 0.1 g of ES and

12.5 ml of the tween to a CS solution and Solution III (Vit D/ES/CS): obtained by mixing 0.1 g of ES, 12.5 ml of tween and 0.75 mg of Vit D with CS solution.

Fabrication of hybrid scaffolds

Three different scaffolds including CS, ES/CS and Vit D/ES/CS were fabricated in this study using freeze-drying approach. The attained compounds mixed for a few hours and poured into plates. The plates incubated at 20 °C for 12 h at –70 °C for 72 h. After this time, the plates covered with aluminum foil and placed in a freeze dryer to dry. Then the synthesized scaffolds were characterized in terms of their chemical and biological properties.

Materials characterization

Scanning electron microscopy

The morphology and uniformity of the scaffolds were analyzed by field emission scanning electron microscopy (FESEM; Philips XL30; Philips, Eindhoven, Netherlands). FESEM was used with the accelerated voltage of 25 kV and after sputtering a 5 nm gold layer on the samples.

Fourier transformed infrared spectroscopy

FTIR was conducted according to ASTM E168-06 [11] and ASTM E1252-98 [12] standards, using a Bruker, Equinox55 spectrometer (Bruker, Equinox55 spectrometer, US) over the scanning range 500–4000 cm^{-1} with a resolution of 2 cm^{-1} .

X-ray diffraction

XRD patterns were obtained on a D/Max BR diffractometer (Riga Ku, Tokyo, Japan) with Cu K α radiation (40 mV/30 mA) over the 2 θ range 5–60°, according to ASTM 1508 standard [13].

Cytocompatibility and in vivo evaluation of scaffolds for the wound healing process

MTT assay

L929 fibroblast cell line was obtained from the Pasteur Institute cell bank (Tehran, Iran). The 7×10^3 L929 human fibroblasts were seeded on each sample in a 48-well plate. The cells were cultured in the cell culture medium (RPMI) (Sigma-Aldrich, US) supplemented with 10% FBS and 1% penicillin–streptomycin (Invitrogen Co, US) at 37 °C under 5% CO₂. Then the cell viability of three fabricated scaffolds including CS, ES/CS and Vit D/ES/CS was determined based on ISO 10,993–5:2009 [14], using 3-(4, 5-dimethyl-thiazol-2-yl)-2, 5-diphenyltetrazolium bromide (MTT) (Sigma-Aldrich, US) assay after 24 and 48 h. In this assay, the supernatants of the

wells were replaced with 10 λ of MTT solution (5 mg/ml diluted with PBS) and 90 λ of the RPMI medium without PBS and corresponding cells. After incubation for 4 h at 37 °C under 5% CO₂, the supernatant was removed and 100 λ of DMSO was added; after shaking or pipetting (5 min), the plates were read in an ELISA (URIT-660, China) reader at a wavelength of 570 nm and a reference wavelength of 630 nm. For measurement the cell viability, the following equation was used: Cell viability = (absorbance of each test well/absorbance of control well) \times 100. Finally, the standard curve was plotted using the values of absorbance read at this stage of the experiment.

Condition of laboratory animals

In the current research 24 male rats weighing 30–35 g were ready and transported to the section of the animal laboratory. Under standard conditions including light & dark period (12/12 h) and a monitored temperature (22–28 °C), the animals were kept. To reduce the undesirable effects of the resulting stress of strange surroundings, the animals had a week period of adaptation before starting the experiment. The rats had free access to water and food and as well as they have been fed with pellets.

Scarring and anesthesia

The rats anesthetized based on the ethical considerations (registered at ethical committee of Shahid Beheshti University of Medical Science NO. IR.SBMU.REC.1396.239) by injecting 0.05 ml of ketamine and xylazine and two full thickness wounds each rat with a diameter of 1 cm using a punch created on the back of the rats.

Groups categorizing

The rats are divided into four groups. The contents of the bandage in different groups were A (ES/CS), B (Vit D/ES/CS), C (CS) and E (standard or commercial). The wounds examined on days 3, 7 and 14 for histology to study the extent of their healing under different scaffolds.

Histopathological examinations

To perform histological examinations, microbial slides first prepared using the following steps: 1. Tissue passage: This step performed using a Tissue Processor device and during the fixing, dehydrating, clearing, floating and molding steps. 2. Molding: In this step, a regular paraffinized tissue molded after the tissue passage step. 3. Cross-sectioning: A microtome used to prepare 5- μ sections, 4. Staining: a) Hematoxylin and Eosin staining: to examine the percentage of the healing; b) Masson's trichrome staining: to evaluate the collagen production.

Evaluation of TGF-β1 gene expression

On the seventh day after inducing the wound, the wound and healed tissue samples taken from the rats and then the enzymatic and mechanical digestion of the tissue samples performed to obtain a single cell. For evaluating the expression of the TGF-β1 gene based on ISO 20,395:2019 [15], the triazole test kit (Sinagene, Iran) used to extract RNA from tissues. To control the quality and to determine the degree of purity and concentration of RNA samples, their optical density (OD) read at the wavelengths of 260–280A and 230/260A using a Bio-Photometer device. In order to determine the expression pattern of the desired genes by existing qualitative and quantitative methods, the RNA extracted from the tissue used to produce the cDNA using a kit. The extracted RNA in the previous step contained various RNA types including mRNA, rRNA and tRNA. Given that one of the properties of the mRNA is the poly-A tail, cDNA constructed using oligo (dT) primer and reverse transcriptase. The inhibitors of ribonucleosides activity also used at this stage.

In order to conduct the real-time PCR process, the materials mixed in a 0.2-ml microtube. The sequence of selected primers was shown in Table 1.

The gene expression ratio in this study evaluated using a comparative method of the threshold cycle (CT). By using the data in Eq. 2, a standard curve specific to the gene plotted using at least five logarithmic concentrations of the diluent, respectively, from the positive control of each gene.

Equation (2):

$$R = 2^{-(\Delta\Delta CT)}$$

$$\Delta\Delta CT = (CT_{target} - CT_{reference})_{TimeX} - (CT_{target} - CT_{reference})_{Time0} \tag{2}$$

The target gene expression level normalized with reference gene and the expression of genes in the healthy group are considered as a calibrator.

Equation (3):

$$Ratio = \frac{(E_{target})^{\Delta CT_{target}}}{(E_{reference})^{\Delta CT_{reference}}} \tag{3}$$

$$(\Delta CT_{reference} = Ct_{control} - Ct_{treatment}, \Delta CT_{target} = Ct_{control} - Ct_{treatment})$$

where, E shows the efficiency and is obtained using the standard curve for the gene.

Table 1 The sequence of used primers

Primers	Sequence
TGF-β1—Forward primer	AAG-AAG-TCA-CCC-GCG-TGC-TA
TGF-β1—Reverse primer	TGT-GTG-ATG-TCT-TTG-GTT-TTG-TCA
GAPDH—Forward primer	CTG-CAC-CAC-CAA-CTG-CTT-AC
GAPDH—Reverse primer	CAG-AGG-TGC-CAT-CCA-GAG-TT

Statistical analysis

The difference between groups was analyzed using GraphPad-online (<http://www.graphpad.com/quickcalcs>). Experiments were repeated three times and all of the data were reported as the mean \pm SD. The results were compared among different groups using a simple one-way ANOVA analysis of variance and Tukey's test ($P < 0.05$).

Results and discussion

Materials characterization

The present study utilized three different techniques for investigating the structure of the synthesized scaffolds. The electron microscope image of the composite Vit D/ES/CS scaffold is shown in Fig. 1. The analysis of the FESEM image for combined scaffold explains highly homogeneous structure as the components have been well arranged in terms of the size and the distance between them. Also, it is clearly seen that this scaffold has porous form and the pores are interconnected. The porosity of scaffolds is a critical factor for using in tissue engineering. Scaffolds must have adequate porosity to facilitate the harboring of cells, cell penetration and migration, tissue ingrowth, vascularization, nutrient supply and gas exchange within the targeted area [16]. In a previous study also a porous chitosan sponge was prepared by the controlled freezing and lyophilization method and the fabricated chitosan scaffolds had a typical microporous structure, with the pore size ranging from 50 to 200 μm [17]. They showed that the chitosan scaffold has sufficient porosity and can prepare a large area of internal surface for cell attachment and migration and can also facilitate the exchange of nutrients

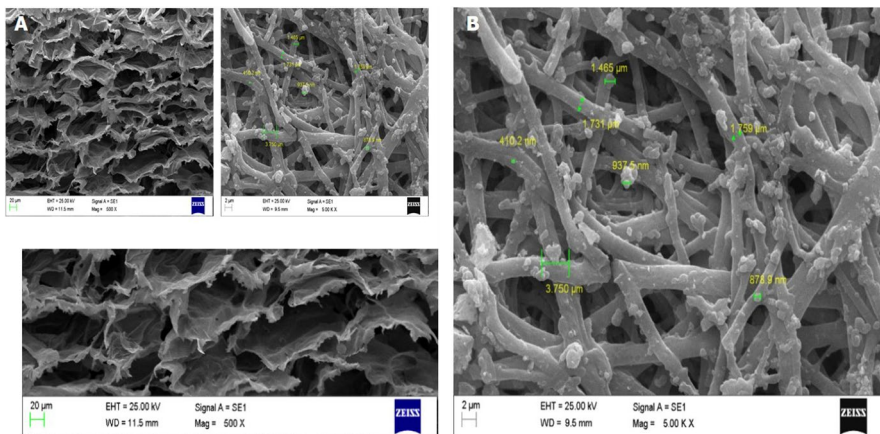


Fig. 1 Representative SEM images of CS/ES/Vit D composite scaffold. **a** The microscopic structure of scaffold. **b** The size of particles forming the scaffold, (CS: Chitosan, ES: egg shell, Vit D: vitamin D)

and metabolic waste. Another noteworthy point about the characteristics of this scaffold as shown in Fig. 1 is the roughness of the walls of the scaffold due to the present of ES particles and Vit D, which will contribute cell adhesion and spreading. Also, as shown in Fig. 1, the synthesized scaffold has a coherent and uniform structure that also fits with the data from FT-IR and XRD. Images with larger magnifications for these scaffolds showed the nano-scale size of the components.

FT-IR analysis is performed to characterize the functional groups of ES, CS, vitamin D and CS/ES/Vit D scaffold, which is shown in Fig. 2. The FT-IR spectral in Fig. 2a shows that calcium phosphates were formed on the surface of ES fibers (in correlation with the XRD results), including hydroxyapatite. All spectra contain the characteristic peaks at 966, 1018 and 1083 cm^{-1} for phosphate stretching vibration modes of PO_4^{3-} [18]. The peak in 1419 cm^{-1} can be related to the existence of carbonate minerals within the eggshell matrix [19]. The appeared peak at 3565 cm^{-1} may be associated with the presence of amino functional groups and hydroxyl (O–H) stretching mode [20].

As shown in Fig. 2b the important bands of CS are as follows. The appeared band at around 3415.31 cm^{-1} can be related to the stretching vibration of O–H and N–H. The existence of residual N-acetyl groups was determined by the bands at around 1645 cm^{-1} (C=O stretching of amide I) and 1325 cm^{-1} (C–N stretching of amide III), respectively. The presence of bands at around 1423 and 1384 cm^{-1} confirmed the CH_2 bending and CH_3 symmetrical deformations, respectively. The band in the range 1157 cm^{-1} to 896.25 cm^{-1} indicates the particular absorb peaks of β -1,4 glycoside bond in chitosan [21, 22]. Chhabra et al. studied the optimization and effectiveness of 2% CS for tissue engineering and wound healing

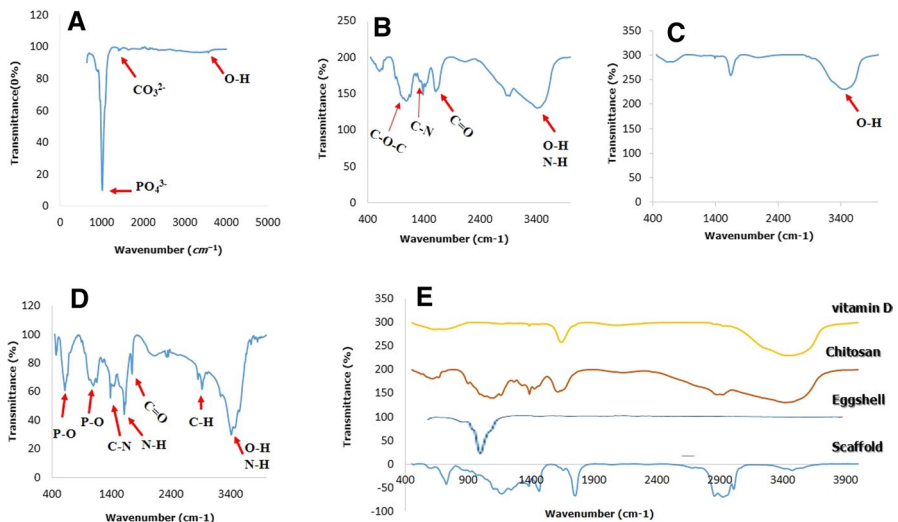


Fig. 2 FTIR spectrum of different biomaterials. **a** ES; **b** CS; **c** Vitamin D/ES **d** CS/ES/Vit D composite scaffold, **e** FT-IR spectra of scaffold component and their combination, (CS: Chitosan, ES: egg shell, Vit D: vitamin D)

and investigated the CS scaffold structure using the FT-IR spectrum; the results observed in the FT-IR spectrum analysis were similar to the present research [23].

FT-IR spectra of combination of vitamin D with ES is shown in Fig. 2c. The represented absorption lines in the regions of 1637 and 1530 cm^{-1} associate with Amide I and Amide II, respectively. The observable peak at 3463 cm^{-1} belongs to the hydroxyl group indicated by the O–H stretch [24].

The FT-IR spectra for CS/ES/Vit D composite scaffold was represented in Fig. 2d. The main aim of this assessment is indicated through the identification of all chemical composition in the ultimate product, along with establishing the probable interactions among their characteristic functional groups. The intense peak in 3412.61 cm^{-1} in this composite scaffold is related to the stretching vibration of O–H and N–H, which hydroxyl group exists in all components of the composite scaffold. The bond from 2922.25 cm^{-1} associates with C–H stretching mode and the bonds from 1383.74, 1551.11 and 1636.44 cm^{-1} , which demonstrate amide III (C–N), amide II (N–H) and amide I (C=O) groups, have undergone a reduction in absorption in the biocomposite, significantly due to the combination with the inorganic phase, decreasing part of the signal [20]. The calcium phosphates (including hydroxyapatite) are also characterized in the composite scaffold and determined via their specific bands around 1053 and 618 cm^{-1} , associate with the P–O bond [19].

The present study used for the first time a composite scaffold CS/Vit D/ES for rapid wound healing. As shown in Fig. 2e, the peaks obtained in the combination of the scaffold component spectra also exist in the FT-IR spectra obtained from the CS/ES/Vit D composite scaffold, indicating well-combined components of the scaffold to form a uniform structure.

The XRD spectrum of the CS, ES and CS/ES/Vit D samples is shown in Fig. 3. According to the XRD spectrum of the ES (Fig. 3a), hydroxyapatite ($\text{Ca}_{10}(\text{PO}_4)_6(\text{OH})_2$) was formed from eggshells source calcium carbonate. The hydroxyapatite is observed clearly defined and highly crystalline hexagonal structure with no evidence of any secondary phase formation, showing the peaks with the intensities of $2\theta = 25.92^\circ$, 31.85° , 32.9° , 49.53° [25]. Comparison of the obtained XRD spectrum with other studies showed a similarity between them. Kumar et al. in a study convert the ES to the hydroxyapatite nanostructure for biomedical applications. They used the XRD spectrum to analyze the ES structure, similar to those of the present study [17]. Prabakaran et al. used an XRD spectrum to develop calcium phosphate-based apatite from ES, whose findings were consistent with the results viewed in the present study [18]. In addition, in the CS XRD spectrum, a peak is visible at the angle of $2\theta = 20^\circ$ (Fig. 3b). The resulting spectrum is similar to the XRD spectrum published in previous studies. In the studies of Huang et al. to investigate the electrochemical effect on the reaction of hydroxyapatite in CS scaffold porous [19] and Ma et al. to prepare and characterize water-soluble N-alkalized CS [20]; as well as Singh et al. to investigate the increased synthesis of CS-graft-polyacrylamide with microwave, the XRD spectra were used to investigate the chemical structure of CS. Their results were similar to the results obtained in this study. In general, the peaks in the XRD spectrum represent a crystalline structure. In the present study, reduction in the intensity of peaks found on the XRD spectrum of the synthesized CS/ES/Vit D scaffold (Fig. 3b), showing the polymer structure and

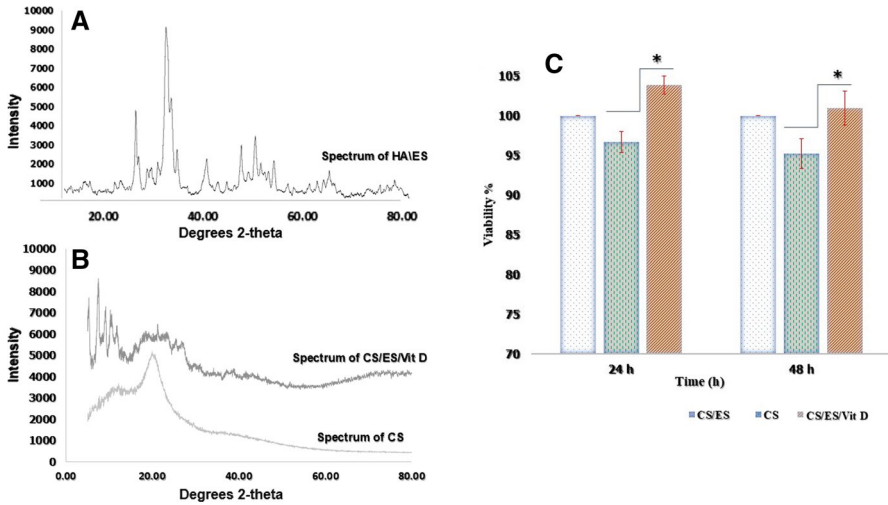


Fig. 3 XRD spectra of scaffold components. **a** XRD spectrum of hydroxyapatite obtained from eggshell (HA/ES). **b** XRD spectrum of CS and CS/ES/Vit D scaffold. **c** Comparing the viability of fibroblasts cultured on CS, CS/ES and CS/ES/Vit D scaffold. Cell viability on the scaffold (CS/ES/Vit D) was significantly higher than the CS group in 24 and 48 h after culture time ($P < 0.05$). (CS: Chitosan, ES: egg shell, Vit D: vitamin D)

decreased crystallinity rate of the composite scaffold. It can be assumed that the scaffold components well combined, interact together and form a homogeneous polymer structure. From the results of FT-IR, XRD and FESEM, it can be concluded that the synthesized scaffold has a homogeneous and polymer structure and there may be some interactions between its components.

Evaluation of fibroblast cell viability

As shown in Fig. 3c, the fibroblasts cultured on CS/ES/Vit D scaffold had more viability than when cultured on CS. The test performed after 24 and 48 h and the viability of the fibroblasts grown on the Vit D/ES/Cs was significantly higher than the CS in both periods. Earlier, Ueno et al., Chen et al., Minagawa et al. and Chhabra et al. showed that CS increased fibroblast cells in the wound and were not cytotoxic for these cells [23, 26–28]. These findings were consistent with the findings of the present study. In addition, in our study, it was first found that the synthesized scaffolds from the combination of CS, vitamin D and ES are far more effective than chitosan. Also, in a recent study by Neacsu et al. hydroxyapatite (ES)–gelatin–bone ash–CS composite scaffold was prepared and amniotic fluid stem cells were cultured on it [20]. The results of the MTT assay showed that the synthesized scaffold stimulates cellular proliferation and this is likely due to the bioactive nature of the added calcium phosphates, coupled with the high surface area provided by the porous structure of the scaffolds. In the analysis of MTT data (Fig. 3c), the viability of the fibroblasts decreased after 48 h compared to 24 h when fibroblasts cultured on both

composite scaffold and CS, as this can be attributed to the conversion of fibroblastic cells to fibrocytes, which is essential for collagen production [29]. Therefore, the results indicate that fibroblasts have been converted to fibrocyte with extend the culture time and that conditions for collagenization have been well prepared.

Histopathological observations

Hematoxylin–Eosin and Masson’s trichrome staining

After assessment of the biocompatibility of scaffolds, the effect of Vit D/ES/CS on wound healing *in vivo* was investigated using a murine full-thickness skin defect wound model. Regarding the images of H & E-stained tissues for evaluating the epithelialization, in all experimental groups, the epithelial layer was not formed on the third day, but on the seventh and fourteenth days, the epithelium began to build and expand. On the seventh day, the epithelialization in group C treated with CS was higher than in other groups. Combine ES/CS (group A) also showed a high ability to produce epithelium and was almost the same as CS. However, the scaffolds synthesized with Vit D/ES/CS (group B) and standard samples (group E) had less ability to create epithelium than the previous two groups. On the 14th day, the results showed that epithelialization was highest in ES/CS group and the lowest in standard samples (Fig. 4). The topic of interest in this study, which was studied for the first time, was that all synthesized scaffolds (CS, CS/ES and Vit D/ES/CS groups) significantly increased epithelialization ($P < 0.05$) compared to the standard group, highlighting the positive activity of CS/Vit D/ES scaffold in wound healing. Epithelialization comparison chart in different experimental groups is shown in Fig. 6a.

Also, according to the results of Masson’s trichrome staining, it was shown that on the 7th and 14th days, the collagenization occurred in all rats, with the difference that the collagen tissue formed in the treatment groups had a more regular and normal arrangement compared to the untreated group. In untreated tissue, the collagen had no distinct boundary between skin layers and only a large amount of collagen was observed (Fig. 5). On the 14th day, collagen production in ES/CS and CS/Vit D/

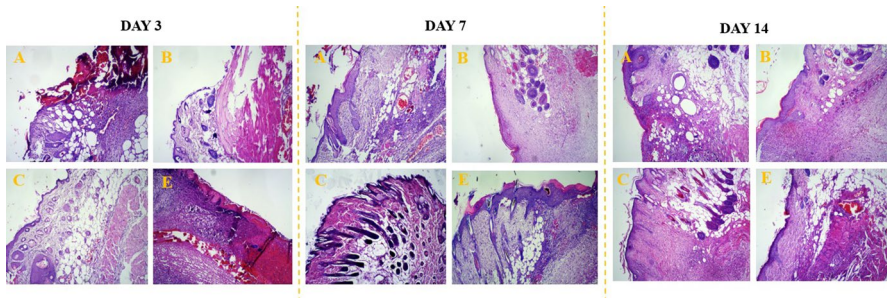


Fig. 4 Images of H & E-stained tissues for comparison of epithelialization percentage on days 3, 7 and 14 after surgery, in the four tested groups: **a** (ES/CS), **b** (Vit D/ES/CS), **c** (CS) and **e** (standard), (CS: Chitosan, ES: egg shell, Vit D: vitamin D)

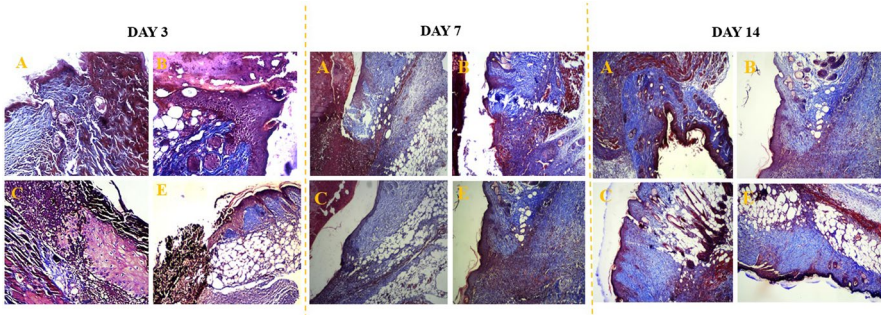


Fig. 5 Images of Masson's trichrome stained tissues for comparison of collagenization percentage on **a** (ES/CS), **b** (Vit D/ES/CS), **c** (CS) and **e** (standard) groups in 3, 7 and 14 days after surgery, (CS: Chitosan, ES: egg shell, Vit D: vitamin D)

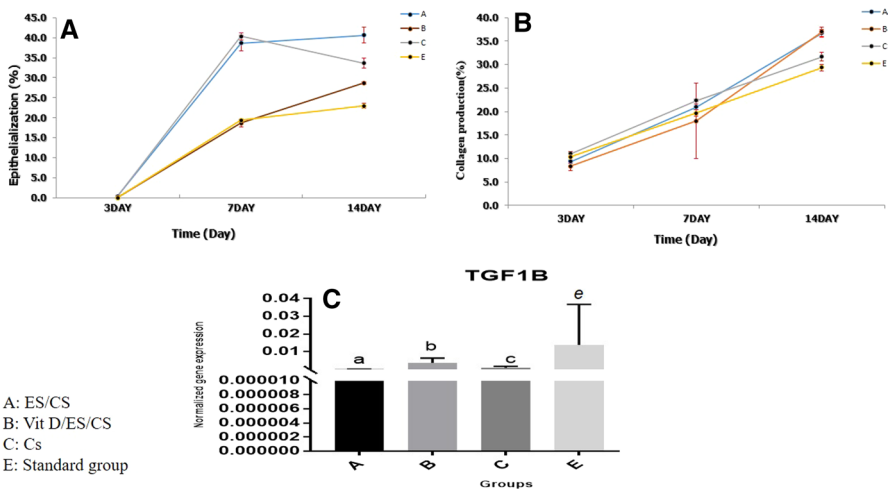


Fig. 6 Comparison of wound healing rate in different groups: **a** Comparison of epithelialization in different experimental groups and in different days: all synthesized scaffolds (groups A, B and C) significantly increased epithelialization ($P < 0.05$) compared to the standard group (E), **b** Comparison of collagenization percentage in different experimental groups and in different days: Collagen tissue formed in the treatment groups had a more regular and normal arrangement compared to the standard group; **c** Evaluation of TGF- β 1 gene expression using Real-Time PCR in seventh day; A (ES/CS), B (Vit D/ES/CS), C (CS) and E (standard), (CS: Chitosan, ES: egg shell, Vit D: vitamin D)

ES groups is higher than other groups. Collagenization comparison chart in different experimental groups is shown in Fig. 6b.

Epithelialization is the hallmark of the healing process used as a determinative factor of a successful wound closure. A wound cannot be significantly healed in the absence of re-epithelialization [30]. Also, collagen plays an important role in each phases of wound healing process due to its chemotactic role. It attracts cells such as fibroblasts and keratinocytes to the injured location. This stimulates debridement, angiogenesis and re-epithelialization [31].

The findings in this study were in line with the reports of Azad et al. on the application of the CS membrane as a dressing for wound healing [28]. They served Bactigras, a sterile paraffin Tulle Gras dressing as a control. They showed that mesh chitosan membrane caused ooze blood into the surrounding gauze. After 10 days, the chitosan-dressed area had been healed more quickly as compared with the Bactigras dressed area. Besides, the chitosan mesh membrane indicated a positive effect on the re-epithelialization and the regeneration of the granular layer. Therefore, they showed that chitosan mesh membrane can be a promising substitute for human wound dressing. In another study, Liu et al. synthesized a wound dressing consists of an optimized concentration of silver nanoparticles (AgNPs) incorporated into the microfibers of a natural eggshell membrane (EM) using mussel-inspired dopamine [32]. In a murine full-thickness skin wound model, they found that EM/AgNPs could stimulate re-epithelialization, granulation tissue formation and wound healing via elevating cell proliferation and control inflammation. In another study, Yuan et al. reported that vitamin D supplementation significantly accelerates wound healing of diabetic mice and improves the healing quality [33]. They showed that vitamin D not only reduced the apoptosis rate but also enhanced cell viability in human umbilical vein endothelial cells. Furthermore, the expression of endogenous markers of endoplasmic reticulum stress was down-regulated as a result of vitamin D treatment. Also, vitamin D supplementation improved collagen deposition and caused fully re-epithelialization in ulcer tissues in the normal group. These data confirm the results of our study that the contribution of ES and vitamin D in the chitosan scaffold can considerably improve wound healing in less time.

Evaluation of TGF- β 1 gene expression

TGF- β 1 is an important parameter in cutaneous wound healing. It is produced by macrophages, fibroblasts, keratinocytes and platelets. TGF- β is a multifunctional growth factor that attracts new fibroblasts and macrophages to the wound site, promotes fibroblast proliferation and collagen production, decreases extracellular matrix degradation and modulates the immune system [34]. The TGF- β 1 gene expression was evaluated on the third day in different experimental groups and the results are presented in Fig. 6c. Since the difference in the gene expression level in the different experimental groups on its scale (bottom of Fig. 6c) was not known, so the data at a scale of 10^3 were also examined to make the differences more distinct. The highest TGF- β 1 expression level was in the standard group (group E), followed by subsequently, in group B treated with composite CS/ES/Vit D scaffold and then in the CS (group C) and CS/ES (group A) scaffolds treated groups (Fig. 6c). Regarding these findings, the TGF- β 1 expression level in all experimental groups was not significantly different from that of the untreated N group ($P > 0.05$). As shown in Fig. 6c, given the fact that the graph has a normal distribution, it is possible to ensure test accuracy. The results of Chen et al. and Jiang et al. have shown that the CS increases the TGF- β 1 expression level [35, 36], while Tsai et al. stated that the CS could inhibit the TGF- β 1 expression [37].

Conclusion

In the present study, the combination of CS, ES and vitamin D resulted in a homogeneous and polymeric scaffold which able to enhance the viability of fibroblasts, the epithelialization and collagenization at the wound site. All of these are essential and useful factors on the wound healing process. Therefore, it can be concluded that the synthesized composite scaffold can improve and accelerate the wound healing process and can replace some of the wound healing chemicals as a natural substance. Studies in this field require further testing and research to achieve a standard combination of the scaffold components.

Acknowledgment We gratefully acknowledge the Proteomics Research Center, Shahid Beheshti University of Medical Science for financial support (Grant NO: 12821).

Compliance with ethical standards

Conflict of interest No potential conflict of interest was reported by the authors.

Ethical approval Ethical approvals for this study was given by Shahid Beheshti University of Medical Sciences (registered at ethical committee of Shahid Beheshti University of Medical Science NO. IR.SBMU.REC.1396.239).

References

1. Akbik D, Ghadiri M, Chrzanowski W, Rohanzadeh R (2014) Curcumin as a wound healing agent. *Life Sci* 116(1):1–7
2. Wang X-J, Han G, Owens P, Siddiqui Y, Li AG (2006) Role of TGF β -mediated inflammation in cutaneous wound healing. In: *Journal of Investigative Dermatology Symposium Proceedings*. vol 1. Elsevier, pp 112–117
3. Duffy SK, Rajauria G, Clarke LC, Kelly AK, Cashman KD, O'Doherty JV (2017) The potential of cholecalciferol and 25-hydroxyvitamin D3 enriched diets in laying hens, to improve egg vitamin D content and antioxidant availability. *Innov Food Sci Emerg Technol* 44:109–116
4. Toiserkani H, Sadaghat F (2013) Chitin and chitosan: structure, properties and applications. *Journal of Aquatic Ecology* 2(3):40–26
5. Fahmy M, Jazayeri H, Razavi M, Hashemi M, Omid M, Farahani M, Salahinejad E, Yadegari A, Pitcher S, Tayebi L (2016) Biomedical Applications of intelligent nanomaterials. *Intelligent Nanomaterials* 199:245
6. Sinha T, Ahmaruzzaman M (2015) High-value utilization of egg shell to synthesize silver and gold–silver core shell nanoparticles and their application for the degradation of hazardous dyes from aqueous phase-A green approach. *J Colloid Interface Sci* 453:115–131
7. Siregar R, Al-Baarri A, Hintono A, Pramono Y, Abduh S (2016) Purification and protein analysis of ovotransferrin from eggshell membrane of local Indonesia and leghorn hens. *Jurnal Teknologi dan Industri Pangan* 27(1):87–94
8. Kozuka M, Murao S, Yamane T, Inoue T, Ohkubo I, Ariga H (2015) Rapid and simple purification of lysozyme from the egg shell membrane. *J Nutr Sci Vitaminol (Tokyo)* 61(1):101–103
9. Khanmohammadi M, Khoshfetrat AB, Eskandarnezhad S, Sani NF, Ebrahimi S (2014) Sequential optimization strategy for hyaluronic acid extraction from eggshell and its partial characterization. *J Ind Eng Chem* 20(6):4371–4376

10. Crisp M, Demarchi B, Collins M, Morgan-Williams M, Pilgrim E, Penkman K (2013) Isolation of the intra-crystalline proteins and kinetic studies in *Struthio camelus* (ostrich) eggshell for amino acid geochronology. *Quat Geochronol* 16:110–128
11. International A (2006) ASTM E168–06 Standard Practices for General Techniques of Infrared Quantitative Analysis. ASTM International West Conshohocken, PA
12. ASTM E1252–98, Standard Practice for General Techniques for Obtaining Infrared Spectra for Qualitative Analysis, ASTM International, West Conshohocken, 2013, pp. 1–13.
13. E-12 A (1998) Standard Guide for Quantitative Analysis by Energy-Dispersive Spectroscopy. ASTM International
14. ISO D (2009) 10993–5: 2009—Biological Evaluation of Medical Devices—Part 5: Tests for in vitro Cytotoxicity (ISO 10993–5: 2009). German Version
15. ISO. Biotechnology — Requirements for evaluating the performance of quantification methods for nucleic acid target sequences qPCR and dPCR. ISO 20395:2019(en). <https://www.iso.org/obp/ui#iso:std:iso:20395:ed-1:v1:en>
16. Armentano I, Dottori M, Fortunati E, Mattioli S, Kenny J (2010) Biodegradable polymer matrix nanocomposites for tissue engineering: a review. *Polym Degrad Stab* 95(11):2126–2146
17. Ikeda T, Ikeda K, Yamamoto K, Ishizaki H, Yoshizawa Y, Yanagiguchi K, Yamada S, Hayashi Y (2014) Fabrication and characteristics of chitosan sponge as a tissue engineering scaffold. *BioMed research international* 2014
18. Apalangya V, Rangari V, Jeelani S, Dankyi E, Yaya A, Darko S (2018) Rapid microwave synthesis of needle-like hydroxyapatite nanoparticles via template directing ball-milled spindle-shaped eggshell particles. *Ceram Int* 44(6):7165–7171
19. Berzina-Cimдина L, Borodajenko N (2012) Research of calcium phosphates using Fourier transform infrared spectroscopy. *Infrared Spectroscopy-Materials Science, Engineering and Technology* 12(7):251–263
20. Neacsu IA, Serban AP, Nicoara AI, Trusca R, Ene VL, Iordache F (2020) Biomimetic composite scaffold based on naturally derived biomaterials. *Polymers* 12(5):1161
21. Ma Z, Wang W, Wu Y, He Y, Wu T (2014) Oxidative degradation of chitosan to the low molecular water-soluble chitosan over peroxotungstate as chemical scissors. *PLoS ONE* 9(6):e100743
22. Fernandes Queiroz M, Melo KRT, Sabry DA, Sasaki GL, Rocha HAO (2015) Does the use of chitosan contribute to oxalate kidney stone formation? *Mar Drugs* 13(1):141–158
23. Yarahmadi M, Fakhar M, Ebrahimzadeh MA, Chabra A, Rahimi-esboei B (2016) The anti-giardial effectiveness of fungal and commercial chitosan against *Giardia intestinalis* cysts in vitro. *J Parasit Dis* 40(1):75–80
24. Simana E, Simian R, Portnoy S, Jaffe A, Dekel B (2015) Feasibility Study-Vitamin D loading determination by FTIR-ATR. *Информационно-управляющие системы* (3 (76))
25. Sattary M, Khorasani MT, Rafienia M, Rozve HS (2018) Incorporation of nanohydroxyapatite and vitamin D3 into electrospun PCL/Gelatin scaffolds: The influence on the physical and chemical properties and cell behavior for bone tissue engineering. *Polym Adv Technol* 29(1):451–462
26. Ueno H, Yamada H, Tanaka I, Kaba N, Matsuura M, Okumura M, Kadosawa T, Fujinaga T (1999) Accelerating effects of chitosan for healing at early phase of experimental open wound in dogs. *Biomaterials* 20(15):1407–1414
27. Chen X-G, Wang Z, Liu W-S, Park H-J (2002) The effect of carboxymethyl-chitosan on proliferation and collagen secretion of normal and keloid skin fibroblasts. *Biomaterials* 23(23):4609–4614
28. Azad AK, Sermsintham N, Chandrkrachang S, Stevens WF (2004) Chitosan membrane as a wound-healing dressing: Characterization and clinical application. *Journal of Biomedical Materials Research Part B: Applied Biomaterials: An Official Journal of The Society for Biomaterials, The Japanese Society for Biomaterials and The Australian Society for Biomaterials and The Korean Society for Biomaterials* 69(2):216–222
29. Quan TE, Cowper S, Wu S-P, Bockenstedt LK, Bucala R (2004) Circulating fibrocytes: collagen-secreting cells of the peripheral blood. *Int J Biochem Cell Biol* 36(4):598–606
30. Pastar I, Stojadinovic O, Yin NC, Ramirez H, Nusbaum AG, Sawaya A, Patel SB, Khalid L, Isseroff RR, Tomic-Canic M (2014) Epithelialization in wound healing: a comprehensive review. *Adv Wound Care* 3(7):445–464
31. HOcHsTEiN AO, Bhatia A, (2014) Collagen: Its role in wound healing. *Wound Manage* 4(1):104–109

32. Liu M, Luo G, Wang Y, Xu R, Wang Y, He W, Tan J, Xing M, Wu J (2017) Nano-silver-decorated microfibrillar eggshell membrane: processing, cytotoxicity assessment and optimization, antibacterial activity and wound healing. *Sci Rep* 7(1):1–14
33. Yuan YF, Das SK, Li MQ (2018) Vitamin D ameliorates impaired wound healing in streptozotocin-induced diabetic mice by suppressing endoplasmic reticulum stress. *Journal of diabetes research* 2018
34. Borena BM, Martens A, Broeckx SY, Meyer E, Chiers K, Duchateau L, Spaas JH (2015) Regenerative skin wound healing in mammals: state-of-the-art on growth factor and stem cell based treatments. *Cell Physiol Biochem* 36(1):1–23
35. Chen Q, Lu H, Yang H (2014) Chitosan inhibits fibroblasts growth in Achilles tendon via TGF- β 1/Smad3 pathway by miR-29b. *Int J Clin Exp Pathol* 7(12):8462
36. Jiang K, Wang Z, Du Q, Yu J, Wang A, Xiong Y (2014) A new TGF- β 3 controlled-released chitosan scaffold for tissue engineering synovial sheath. *Journal of Biomedical Materials Research Part A: An Official Journal of The Society for Biomaterials, The Japanese Society for Biomaterials and The Australian Society for Biomaterials and the Korean Society for Biomaterials* 102(3):801–807
37. Tsai C-W, Chiang I-N, Wang J-H, Young T-H (2018) Chitosan delaying human fibroblast senescence through downregulation of TGF- β signaling pathway. *Artificial Cells, Nanomedicine and Biotechnology* 46(8):1852–1863

Publisher's Note Springer Nature remains neutral with regard to jurisdictional claims in published maps and institutional affiliations.